Know the Flow: Non-Contact Magnetic Flow Rate Sensing for Water Meters

Eric A. Ponce, Steven B. Leeb, *Fellow, IEEE*, and Peter A. Lindahl, *Senior Member, IEEE*

***Abstract*—Positive displacement water meters are found throughout the world's water distribution networks to totalize water consumption. Containing internal permanent magnets, the water meters are underutilized sensors. Flow data from these meter locations can be used to non-intrusively identify the operation of individual water loads from an aggregate data stream at the meter. This article models these meters as nonideal magnetic encoders and presents a methodology for inexpensively retrofitting these meters with digital flow rate measurement capabilities, effectively bringing them into the growing body of smart metering devices and non-intrusive load monitoring without any contact with the water passing through them. We present a model of the magnetic field produced by these meters, discuss associated magnetic sensing hardware, and describe compensation, flow rate estimation, and post-processing algorithms for flow rate extraction. Verification is provided with experimental results.**

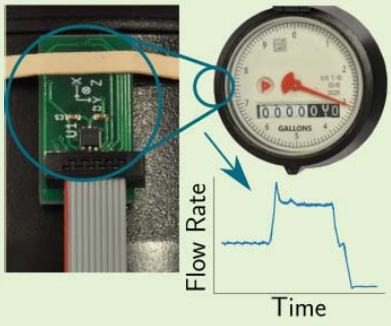

***Index Terms*—Fluid flow measurement, magnetic sensors, sensor data processing, sensor applications.**

I. Know the Flow

HARNESSING the underutilized capabilities of available sensors adds value. This value minimizes the need for excessive sensor installation, networking, and data collation. For example, non-intrusive load monitoring (NILM) provides a window on electrical consumption data without requiring sub-metering of every load of interest [1]. Non-intrusive approaches make better use of fewer sensors, enabling an easier road to automated smart utility grids and metering, distributed management for improved reliability and efficiency, and improved monitoring in resource-constrained environments [2].

Water meters are underutilized sensors. These meters are set at the service entry for fluid connections that may serve a collection of downstream loads. Typical meters totalize consumption but do not report flow. If flow could be measured conveniently, e.g., with a simple retrofit to these existing meters, then flow data could be used to nonintrusively track the operating schedule of the downstream loads. Many existing positive displacement water (PDW) meters use an axially-aligned magnetic coupler to transfer torque from a sealed turbine housing to a metering housing with a totalizer and readout. These magnetic couplers produce a rotating magnetic field that directly corresponds to turbine position. Retrofit, pulse-output attachments for these meters exist, but they lack the necessary resolution at low flow rates to provide reliable non-intrusive flow measurement. The authors of [3] presented a non-contact method for retrofitting existing PDW meters by employing two carefully constructed magnetic field sensors orthogonally placed to recover the rotational angle of the internal magnets. Other methods for recovering water flow rates, such as vibration or acoustic sensors and new, intrusive water metering, along with systems for monitoring these loads, have also been explored [4], [5]. These studies demonstrated the feasibility of NILM techniques and load identification from upstream measurement in water-based networks, bringing along many of the same benefits of non-intrusive monitoring on the electrical system. These works, however, used sensing technologies that were contact-based or invasive to the water network with multiple measurement points, that required careful calibration, or that utilized complex sensors.

This article presents approaches for signal processing and sensing hardware that add functionality to conventional, inexpensive water meters to enable them to serve as high quality flow rate meters. Tailored signal processing algorithms provide flow data that can be read in real-time. Installation is simple, requiring no special skills or sensitive efforts to position

Manuscript received June 24, 2020; revised August 3, 2020; accepted August 4, 2020. Date of publication August 7, 2020; date of current version December 4, 2020. The associate editor coordinating the review of this article and approving it for publication was Prof. Guiyun Tian. *(Corresponding author: Eric A. Ponce.)*

Eric A. Ponce and Steven B. Leeb are with the Department of Electrical Engineering and Computer Science, Massachusetts Institute of Technology, Cambridge, MA 02139 USA (e-mail: eaponce@mit.edu; sbleeb@mit.edu).

Peter A. Lindahl was with the Department of Electrical Engineering and Computer Science, Massachusetts Institute of Technology, Cambridge, MA 02139 USA. He is now with Exponent, Inc., Natick, MA 01760 USA (e-mail: plindahl@exponent.com).

Digital Object Identifier 10.1109/JSEN.2020.3014843

sensors or modify the existing meter. Quality flow data can serve as the foundation for non-intrusively identifying the operation of individual water loads from an aggregate data stream at the meter [3], [6].

In essence, this article examines the water meter from the perspective of a nonideal magnetic encoder. A retrofit solution minimizes cost and installation effort with thoughtful signal processing. We first develop an analytic model for the field produced by the magnetic coupler internal to the meter. This model reveals that the "nonideal" field produced by the magnetic coupler can be exploited to simplify sensor installation. Specifically, we use the model to drive sensor placement and to motivate application of a two- or three-axis sensor rather than the two orthogonally placed single-axis sensors used in past work [3], reducing sensor and retrofit cost and effort. We then introduce an example sensing system and present automatic preprocessing algorithms for compensating for flux density and offset differences between PDW meters and field directions. Finally, we explore several signal processing methods for extracting instantaneous flow rates from the meters and verify the performance of these methods with experimental results.

II. Opportunity

Standard residential PDW meters are composed of a turbine housing (TH) and a metering housing (MH), magnetically linked by an internal axially-aligned magnetic coupler. The meter explored in this article uses two axially-polarized multipole disks to form this coupler. The rotating magnets within the meter present an opportunity for detection of the rotation of the positive-displacement turbine and the associated water flow without any contact with the water. The configuration of a rotating permanent magnet and magnetic field sensor, referred to as a magnetic encoder, finds wide use in commercial, industrial, and scientific applications. By attaching a magnetic field sensor to the exterior of the meter, we create a nonideal, but useful, magnetic encoder out of existing meters.

In this section, we first present the physical parameters and working range extracted from an example PDW meter chosen for this investigation: a Neptune 5/8 T-10 Meter [7]. An analytic three-dimensional field model is developed to simulate the field in the space along the exterior of the meter and explore the field characteristics useful for extracting positional information. Finally, we determine the optimal placement of a magnetic field sensor on the exterior of the meter using the results of the simulation.

A. Positive Displacement Water Meter

The PDW meter consists of a totalizer or metering housing for recording water consumption and a turbine housing containing the mechanism that converts water flow to mechanical rotation. The two housings are linked together with a magnetic coupler composed of two four-pole-pair axially-polarized disk magnets and are almost entirely composed of low-permeability polymer and copper materials, except for a cast iron plate sealing the TH. A sacrificial meter was dismantled and its geometric parameters, along with those of the internal magnetic coupler, were measured and summarized in Table I. The

TABLE I
PDW Magnet and Housing Geometric Parameters (mm)

	r_1	r_2	z_1	z_2	r_{in}	r_{out}	z_b	z_p	z_t
D_1 | TH	2.7	11	−7.7	−3.15	89	94	−60	−39	−7.6
D_2 | MH	2.1	7.9	3.2	6.4	76	89	−7.6	11	36

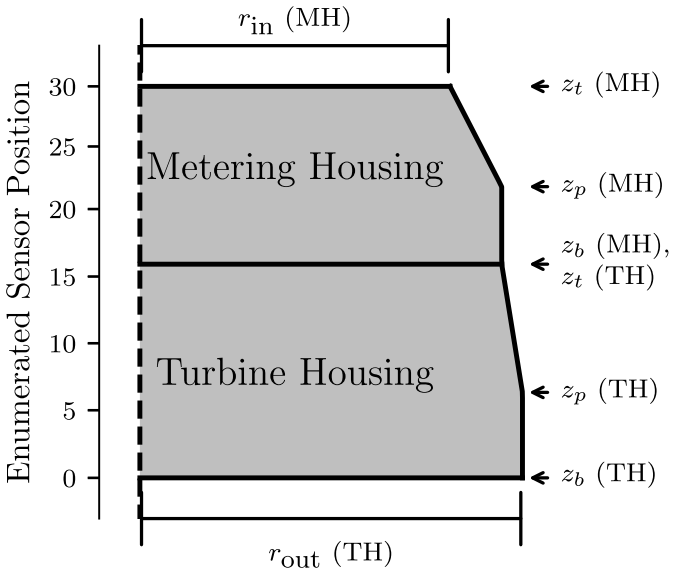

Fig. 1. PDW meter housing geometry.

magnetic disks D_1 and D_2 refer to the magnets within the TH and MH, respectively. Each housing is composed of a cylindrical section followed by a sloped section, allowing each of them to be approximately defined by an inner and outer radius, r_{in} and r_{out}, as well as bottom, pivot, and top positions, z_b, z_p, and z_t, respectively, as shown in Fig. 1.

The American Water Works Association (AWWA) standard operating range of 0.23 to 4.5 $\text{m}^3 \cdot \text{h}^{-1}$ was selected for this investigation and was determined from the product sheet of the meter. However, the algorithms presented later in this work are sensitive to much lower flow rates. This range was used in part for determining the minimum sample rate necessary for digital data acquisition.

B. Magnetic Field Model

The meter, composed of low permeability brass in the TH and plastic in the MH, will produce an exterior magnetic field that is the superposition of the two disk magnets, axially-aligned and spinning together. For the purposes of this article, the two magnetic disks are assumed to have no slip; however, torque-slip models of the axial magnetic couplers can be incorporated into the model for more accurate estimation of the field near the maximum flow rate of the PDW meter as in [8], [9]. The no-slip model produces excellent results here, as the meter is designed to couple reliably and avoid pull-out torque levels even at high flow rates. To model the high-permeability plate sealing the bottom of the TH, the method of magnetic images is used to ensure the magnetic flux boundary conditions on the surface of the plate are maintained.

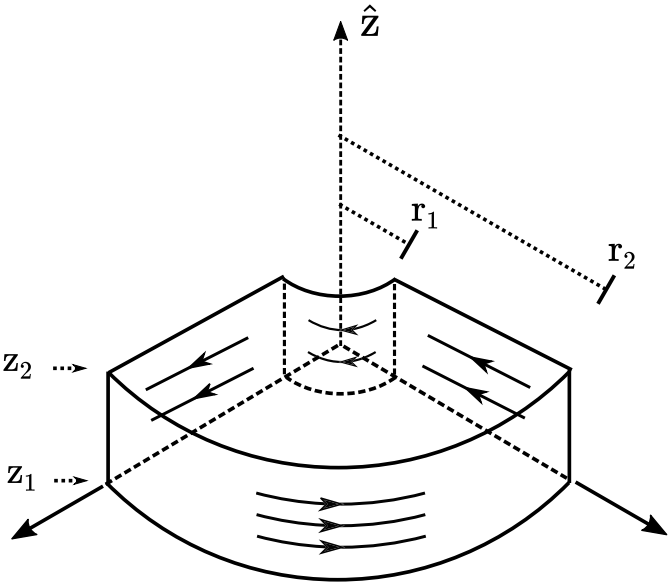

Fig. 2. Cylindrical magnet sector geometry with surface currents for axial polarization.

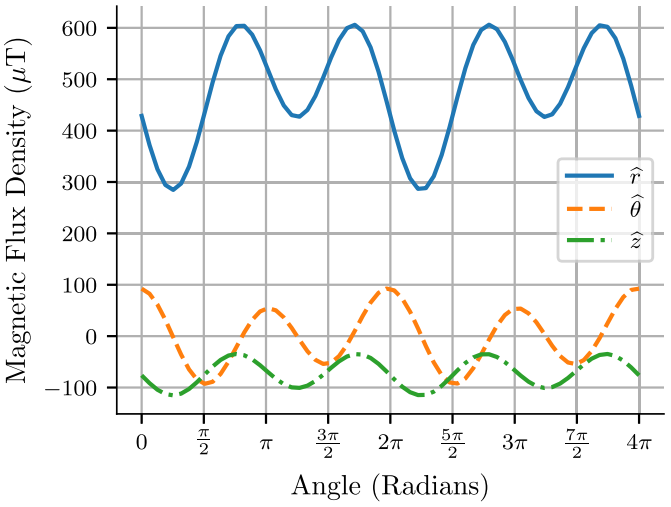

Fig. 3. Simulated PDW coupler over two revolutions.

An individual magnetic disk is divided into p homogeneous, single pole-pair, cylindrical sectors that are modeled using equivalent surface currents running parallel to the direction of polarization, $\hat{z}$, as shown in Fig. 2. Analytical solutions for the magnetic flux density produced by such a cylindrical sector are presented in [10]. Superimposing all sectors for each magnet in the coupler, along with their respective magnetic images, produces an analytic model for the magnetic field around the periphery of the PDW meter.

C. Magnetic Field Simulation

Fig. 3 shows simulated data for this coupler configuration over two revolutions of the magnetic coupler along the top circumference of the MH at $r = r_{in}$ and $z = z_t$. A base magnetization of 13×10^6 A·m^{-1} was used, with asymmetric scaling factors for each pole-pair of $[-1.05, 1.1, -0.8, 1.1]$. This and the analytic solutions to this magnetic coupler's configuration demonstrate that the external field will be non-linear by nature. These non-linearities lead to estimation error in the various flow-rate estimation techniques discussed here, and manifest as extraneous modulation on top of the flow rate. The major sinusoidal component of the field, at a period of $P_{f,a} = \pi$, will be referred to as the field fundamental harmonic (FF) and corresponds to the alternating pole-pairs of the coupler. The second major sinusoidal component of the field, at a period of $P_{m,a} = 2\pi$, will be referred to as the mechanical fundamental (MF) harmonic and results from geometric and/or magnetization asymmetries common in cost-sensitive magnetic coupler construction. They are related by the number of pole-pairs p as $P_{f,a} = s_f P_{m,a} = (2/p) P_{m,a}$.

For the test meter, 60 revolutions of the magnet corresponds to 3.785 L of passing water, resulting in an AWWA-accurate metering range of approximately 2 Hz–40 Hz. In practice, however, frequencies outside of this range are expected, and so a working range of 0.1 Hz–50 Hz was selected, leading to minimum sample rate greater than 100 Hz.

This polarization structure produces a $\hat{\theta}$ component that peaks near the sector's azimuthal boundaries, whereas the other components peak near the azimuthal center of the sector. Thus, as has been found for a variety of multi-pole magnetic encoder topologies [11], these magnets produce a $\hat{\theta}$ field component that is nearly in quadrature with the $\hat{r}$ and $\hat{z}$ components. Thus, a properly aligned two-axis magnetic field sensor can take advantage of these quadrature fields to estimate the phase of the field, and therefore, the position of the magnetic coupler internal to the PDW, with only a single multi-axis magnetic sensor. No special alignment of two physical sensors is necessary to capture two quadrature sinusoids for sensing rotation.

To determine the optimal position for a magnetic field sensor, the FF magnitude of the field over a full rotation of the coupler was calculated and plotted against enumerated evenly-spaced sensor position along the exterior of the meter in Fig. 4. A position of 0 corresponds to the bottom of the TH, while a position of 30 corresponds to the point along the top circumference of the MH, as shown in Fig. 1. While the optimal position will vary by meter manufacturer, sensor selection, and application environment, the plot shows the top circumference of the meter as having the peak magnitude in two orthogonal directions, enabling larger SNR measurements. Thus, this region is used throughout the article for magnetic field measurement.

III. Sensing Hardware and Signal Preprocessing

A. Hall-Effect (HE) Sensor and Measurement Setup

A three-axis MLX90393 HE sensor IC with built-in ADC and digital filtering by Melexis [12] was used to measure the magnetic field external to the PDW meter. Offering low cost, down-to-dc frequency response, and high resolution, this sensor is capable enough to pick up the μT order magnetic fields produced outside the PDW meter [3]. An elastic holds the sensor against the housing as shown in Fig. 5, illustrating the simplicity of the mechanical requirements for this retrofit.

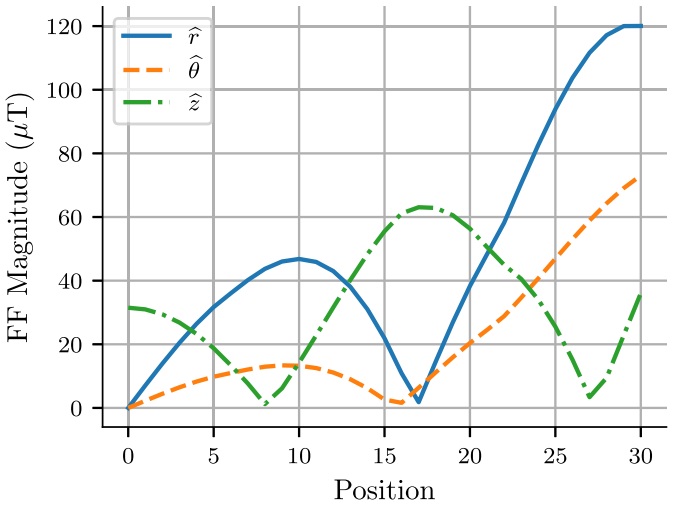

Fig. 4. FF Magnitude along the exterior of the PDW meter housing.

Fig. 5. PDW meter hall-effect sensing setup.

For this particular setup, the highest resolution mode of the HE sensor was used without saturation. The sensor configuration parameters [12] used are: $\texttt{RES\_XYZ} = 0, \texttt{DIG\_FILT} = 2, \texttt{OSR} = 3, \texttt{GAIN\_SEL} = 7$. This results in field sensitivities of $\texttt{SENS\_XY} = 0.150\mu\text{T/LSB}$ and $\texttt{SENS\_Z} = 0.242\mu\text{T/LSB}$, and a sampling rate of $F_s = 127\,\text{Hz}$.

The sensor produces samples in the three component direction $\hat{x}$, $\hat{y}$, and $\hat{z}$. In this case, the two major sinusoidal field directions, $\hat{r}$ and $\hat{\theta}$ in the magnetic couplers reference frame, are in quadrature and correspond to the sensor's $-\hat{z}$ and $-\hat{y}$ directions. The sampled $-\hat{y}$ direction leads the $-\hat{z}$ and so will be referred to as $c_i[n]$, representing the *cosine* term in an analytic signal. The sampled $-\hat{z}$ direction will then be referred to as $s_i[n]$, representing the *sine* term.

Analytic signals formed from quadrature signals contain no negative-valued frequency content. This content serves as a valuable metric for reducing sensor misalignment. For three-axis data, there is a standard rotation matrix [20] that minimizes negative-valued frequency content in the two component directions of interest and can be found using standard minimization and optimization techniques [10]. This serves as a justification for choosing a three-axis sensor over a two-axis sensor, loosening mechanical alignment requirements. We perform this rotation minimization with our data before preprocessing signal streams.

Because we are adding new flow rate sensing functionality to these water meters, a source of reference data is needed for comparison and evaluation purposes. A pulse-output flow rate sensor with a wider operating range for flow detection and a higher resolution than the PDW meter was placed in series with the meter to provide a source of reference flow rate data.

B. Input Preprocessing

Hall-effect sensors and the field produced by real-world magnetic couplers both contain dc offsets, axis sensitivity mismatches, and asymmetric magnetization that lead to errors in phase or angle estimation techniques. Removing field dc bias and scaling amplitudes are the first critical steps to reducing errors and producing initial rotation angle estimates. These characteristics may be compensated for, to a first approximation, by measuring the extremes of the field over a rotation. This approach is susceptible to noise and strong non-linearities [13], as found in the nonideal magnetic encoder formed during the retrofit of PDW meters.

There are several approaches to compensating these parameters when two-axis quadrature data is available. For environments where a reference signal is available, past work has centered around computing correction parameters for use in online compensation to great effect [11], [14], [15], but these references are not available in the retrofit of presently-installed PDW meters. Other work has eliminated the need for a reference signal and relied on computationally expensive iterative searching methods and/or curve fitting [13], [16], [17]. All of these methods depend on using a reference, or an angle estimate, to converge towards optimal compensation parameters. For this work, we have chosen the Harmonic Error Correction (HEC) method, which estimates sinusoidal amplitude and offset parameters for each orthogonal component using an `arctan2`-based angle estimate and a nonlinear observer [18]. This method features stable and fast convergence with low computational and memory requirements, as well as stability during low and no flow periods of operation.

For single-axis data, compensation becomes more difficult as angle estimates are not as easily generated. The simplest methods use a combination of high and low pass filters which impose a requirement for continuous excitation or rotation. Instead, we chose a mixed approach. Amplitude and offset errors are only tracked during periods of excitation determined by the working range of the meter. We determine these periods of excitation with a threshold-based digital asynchronous full-wave envelope detector and then use a high-pass filtered version of the input signal to determine signal extremes on a period-by-period basis. These extremes are passed through a low-pass filter for tracking offsets and amplitudes, a modification of the digital approach found in [19] that works across the entire range of input offsets.

IV. Flow Rate Recovery

The angular position of the magnetic coupler in a PDW meter corresponds directly to the phase of the sensed magnetic

field. The gradient of this phase corresponds to the instantaneous frequency (IF) of the field and therefore the rotational velocity of the magnetic encoder, which linearly relates to the flow rate of water through the PDW meter.

The quadrature pair $(c_i[n], s_i[n])$ measured with the experimental setup may be used to estimate the field's phase and IF. This section presents methods using both these quadrature signals, referred to as two-axis methods, that extract the phase from the FF present in the waveforms.

Cost sensitive applications, may demand a cheaper single-axis sensor. For the purely real signal we measure from a single HE sensor axis, however, the definitions of phase and IF are more tenuous, with phase and frequency no longer being uniquely determined as in the case of an analytic signal [21]. A single real sinusoid has equal power at positive and negative frequencies, leading to ambiguity about the sign of frequency. This section then also presents methods using a single real-valued sinusoid for flow rate estimation.

A. Two-Axis Estimation Methods

A quadrature signal pair can be measured and used to estimate the field's phase and therefore the coupler position. IF estimates may be generated by taking the gradient of the phase estimate or through other methods summarized in [22], [27]. This subsection presents three methods for estimating these parameters. All methods essentially extract the phase from the largest harmonic present in the waveforms, the FF. Higher and lower-order harmonics that were present in the field are modulated on top of the phase estimate, and therefore the IF estimate, when using these methods.

1) Direct Angle Estimator: The HEC compensation method produces amplitude- and bias-corrected orthogonal waveforms, as well as an initial angle estimate. In essence, the rotation angle of the water meter can be estimated directly from the arctangent of the compensated quadrature waveforms. This angle estimate is heavily affected by noise and thus requires extra filtering steps to improve estimates. To estimate the IF from the angle estimate, we start by unwrapping the phase and then low-pass filtering it based on the expected dynamics of the water system. The IF is then computed from the gradient of this unwrapped phase.

2) Kay-Tretter (KT) IF Estimator: As a baseline, and following the work in [3], we implemented the linear Kay-Tretter smoothed phase differencing IF estimator as described in [29].

The algorithm uses a weighted phase differencing window to filter out signal noise and to produce smoother IF estimates. While this approach does well with removing higher-frequency noise, it also assumes a linear change in phase, and thus will also filter out higher-order phase transients. The window size can be tuned to trade off between transient performance and noise rejection, as well as to adjust computation requirements.

3) Digital Quadrature Phase-Locked Loop (DQPLL) Estimator: Following work from [30]–[32], a DQPLL was used to estimate and track the phase $\varphi[n]$ and frequency $f[n]$ of the quadrature signal pair formed from two axes of the field measurement.

As shown in Fig. 6, this DQPLL is composed of a quadrature phase detector (QPD), a proportional-integral loop filter (PILF), and a digital numerically-controlled oscillator (NCO). The QPD estimates the phase difference of the input signals and NCO output by

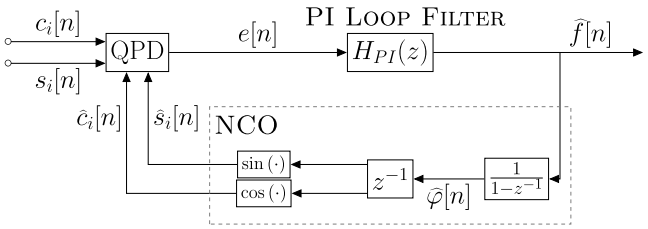

Fig. 6. Digital quadrature phase-locked loop block diagram.

$$e[n] = s_i[n]\cos(\widehat{\varphi}[n]) - c_i[n]\sin(\widehat{\varphi}[n]). \tag{1}$$

This error signal is then passed through a PILF with parameters K_P and K_I and transfer function

$$H_{PI}(z) = \widehat{f}[n]/e[n] = K_P + K_I/(1 - z^{-1}). \tag{2}$$

When locked, the output of the PILF produces an IF estimate $\widehat{f}[n]$ that is integrated in the NCO to generate a phase estimate $\widehat{\varphi}[n]$. The phase estimate is then used to generate two quadrature signals that are fed back into the QPD.

The DQPLL's inner filters result in a cleaner frequency estimate than that produced by direct angle estimation. Tuning K_P and K_I also adjusts the usual PLL properties, allowing one to more accurately track transients in the IF, unlike in the linear KT approach. As is the other approaches that only track the FF, extraneous harmonics in the field result in modulation on the IF estimate.

B. Single-Axis Estimation Methods

One common approach to tracking phase and extracting IF from a single sinusoidal data stream involves taking the Hilbert Transform (HT) of the data to produce an analytic signal containing only positive frequency energy. Due to the intermittent nature of water loads, however, our field signals will often approach dc, at which point the HT will fail to produce a proper analytic signal for IF extraction due to its high-pass nature [22].

The Short-Term Fourier Transform (STFT), another common approach, also suffers from problems related to the periods of no-flow and large IF transients. While the STFT window width generally allows for trading off between time and frequency resolution, the large input signal bandwidth results in an optimal window width for low-flow rates that is much larger than that for high-flow rates [23], [24].

Finally, zero-crossing detection, where the zero-crossing points of the waveform are used to estimate signal period, can be used as a simple estimate of IF. This method is nearly identical to the theory behind pulse-output attachments for meters, where a magnetic reed switch attached to the exterior of the meter produces a pulse at a specific field strength. This allows for low-cost and accurate flow totalizing, where each pulse accounts for a fixed amount of turbine angular displacement. This approach can be performed with our sensor data algorithmically. However, it lacks resolution

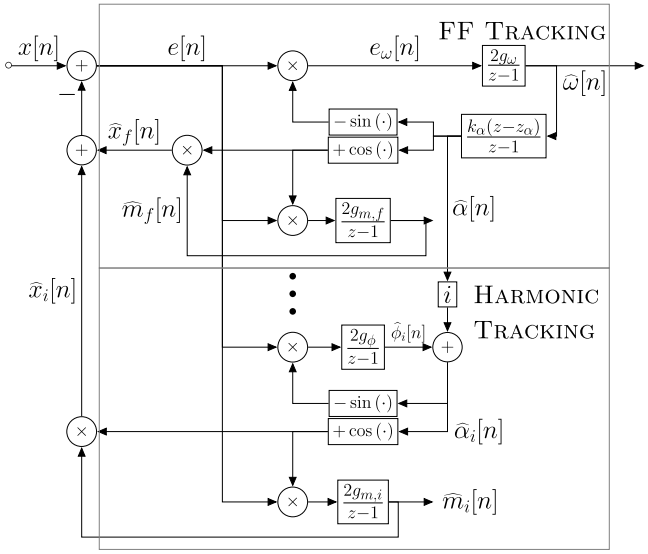

Fig. 7. Harmonic sinusoidal parameter tracker block diagram.

for low-flow flow rate variation as inter-period IF variations will be averaged over a whole period.

The remainder of this subsection describes three methods for estimating flow rates from single-axis sinusoidal data collected from a PDW.

1) Harmonic Sinusoidal Parameter Estimator (SPE): The field solution for an axially-polarized multi-pole magnet demonstrates that there will always be non-linearities in the field that manifest as lower and higher order field harmonics. In particular, for the asymmetric and cost-sensitive magnets within PDW meters, there will be a large harmonic at the MF.

Bodson *et al.* introduce a method for tracking multiple independent sinusoids that uses feedback to estimate the phase and magnitude of each component in [25], [26]. Their approach was discretized and modified so that the SPE tracks the phase, frequency, and magnitude of the FF, while also tracking magnitude and phase offsets of n_h harmonics. In this application, the most important harmonic to track is the MF.

The revised block-diagram is shown in Fig. 7. The estimator produces FF phase $\widehat{\alpha}[n]$, IF $\widehat{\omega}[n]$, and magnitude $\widehat{m}_f[n]$ estimates, as well as n_h harmonic magnitude $\widehat{m}_i[n]$ and phase offset estimates $\widehat{\phi}_i[n]$, where i represents the harmonic phase scaling factor. They are used for generating harmonic estimates $\widehat{x}_i[n]$, which are summed and then subtracted from the input signal $x[n]$.

Due to the ambiguity between positive and negative frequencies in a real-valued sinusoidal signal, the SPE has the potential to momentarily lose track of the frequency, and move towards the negation of that frequency, resulting in a spurious transient. At lower tracking frequencies, the spacing between positive and negative frequencies, $2 \cdot \widehat{f}[n]$, is small, leading to a higher rate of spurious transients. Reducing the frequency update coefficient, g_ω, helps to reduce these spurious transients in the steady-state at the cost of poorer transient performance.

This method, however, with its simple block diagram, is well suited to real-time flow recovery, requiring few operations and memory per sample.

2) Linear Adaptive Prediction Filter (APF): The adaptive linear prediction filter based IF estimator found in analytic form in [27] and proposed by [28] for real signals uses a Least-Mean-Squares (LMS), steepest-descent gradient technique to update prediction coefficients for an all-pole prediction filter (PF) of length p with coefficients $\boldsymbol{H}[n]$ and difference equation

$$\widehat{x}[n] = \sum_{k=1}^{p} h_k[n]x[n-k] = \boldsymbol{H}^T[n]\boldsymbol{X}[n]. \tag{3}$$

Taking the discrete Fourier Transform of the PF coefficients and manipulating the result allows one to generate an estimated time-frequency representation (TFR) with a ridge at the IF for mono-component signals [28] and equation:

$$\widehat{Q}[\omega; n] = \left| 1 - \sum_{k=1}^{p} h_k[n]e^{-j\omega k} \right|^{-2}. \tag{4}$$

Using peak finding algorithms to extract ridges from the TFR allows one to generate an estimate for FF IF, and therefore, find the flow rate.

While [28] chose to use an LMS technique to converge towards the optimal PF coefficients, we found that a Normalized Least-Mean-Squares (NLMS) approach to gradient estimation produced more reliable estimates and improved stability. In the NLMS, the LMS update rate, μ, is normalized as samples are received by

$$\mu_n[n] = \mu/(\epsilon + \boldsymbol{X}^T[n]\boldsymbol{X}[n]). \tag{5}$$

Where ϵ is a positive *regularization* term and $\boldsymbol{X}^T[n]\boldsymbol{X}[n]$ represents the norm of the last p values.

Replacing the update step with a more computationally complex recursive-least-squares technique was also explored in this investigation, but it suffered from poor transient response and noise rejection when compared to NLMS.

After generating the estimated TFR, arbitrary frequency scaling can be used when searching for ridges, with a higher computational cost for searching a bigger space.

3) Continuous Wavelet Transform (CWT): The CWT can be used to generate a TFR of non-stationary waveforms. The choice of wavelet varies the degree of time and frequency localization in the TFR. Nonorthogonal and complex wavelets are best suited for capturing oscillatory behaviors with smooth and continuous variations in parameters [24]. Although this smoothing nature will filter out some transients in our flow, the CWT still serves as a means of generating flow rate estimates. Furthermore, using more complex peak finding algorithms to extract ridges from the TFR may allow future work to better extract features from the flow.

A complex Morlet wavelet, chosen as a time/frequency compromise for general flow rate extraction, has the normalized Fourier transform

$$\widehat{\Psi}(s\omega) = (2s)^{1/2}\pi^{1/4}H(s\omega)\exp^{-(s\omega-\omega_0)^2/2}, \tag{6}$$

where ω_0 is a non-dimensional frequency term used to meet wavelet admissibility conditions for the CWT, $H(s\omega)$ is the Heaviside step function, and s is the scale used during the computation of the CWT.

Scales can be converted to IF estimates through the relation

$$\widehat{f} = F_s(\omega_0 + \sqrt{2+\omega_0^2})/(4\pi s). \tag{7}$$

The relation shows that one would need an infinite scale to emulate frequencies down to dc, limiting our minimum detectable IF. This can, however, remain below the range of proper operation for the PD meter. In addition, the CWT allows for arbitrary resolution along the range of frequencies, unlike the STFT.

Since the CWT relies on convolving the wavelet with the signal, our implementation uses the Fast Fourier Transform and its inverse to improve computational efficiency. This provides significant speed improvements, particularly if the sampled waveform is padded to a power-of-two sample size. Nevertheless, this approach requires high amounts of memory for manipulating the input signals and TFR, which can be reduced at the cost of a higher minimum detectable frequency. As with the APF, however, high frequency-resolution requirements may consume considerable computational resources.

V. Post Processing Flow Rate Estimates

Since almost all the above methods reduce, but do not remove, extraneous field harmonic induced modulation of the phase and IF, a secondary processing step is needed to improve estimates. An FIR moving average filter with window length W, due to the comb-like nature of its frequency response from the windowing procedure, acts like a filter with notches at $\frac{F_s}{W}$ Hz and all higher-order harmonics up to the Nyquist frequency, as well as a low-pass filter for removing higher-frequency noise.

Using the estimates computed in the previous section, a time-varying moving average filter (TVMAF) can be designed, where the window length at sample n is set by the relation

$$W[n] = 1/(s_f \widehat{f}[n]), \tag{8}$$

where s_f is the appropriate scaling factor between the FF and MF spatial periods. By setting the window length to the MF, we reduce the effect of its modulation on top of phase estimates, and all its higher-order multiples. This will induce a time-lag to IF estimates of $F_s/W[n]$ s, which can balloon to infinity for IF estimates of zero, but practical limits on window length can be set to minimize this effect during low-load periods. For the purposes of this article, a maximum window length of 1 s or $W[n] = F_s$, was used.

As the CWT tracks all harmonics in the field simultaneously, it is the only algorithm presented here that did not require a post TVMAF.

After post-processing to remove the extraneous harmonic modulation in IF estimates, the estimate must be scaled from FF IF in Hz to flow rate by using the relation between the FF and MF frequencies, as well as the volume of water per magnetic coupler revolution, both of which may be found in Section II-C.

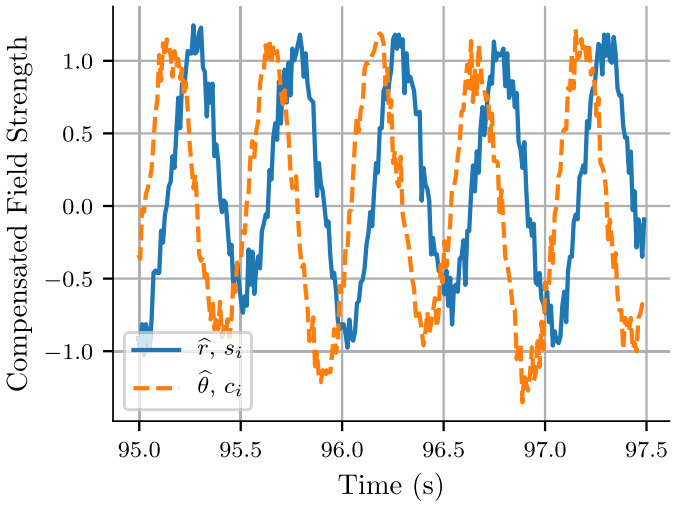

Fig. 8. Sample PDW meter waveforms.

VI. Experimental Results

Sample waveforms from a PDW meter were collected over various steady state load cycles. The two component directions of interest were preprocessed using the single-axis method and are shown in Fig. 8. The waveforms closely correspond to the waveforms predicted by the axial magnetic field solution and demonstrate clear FF and MFs.

For the two-axis methods, direct angle estimation used one output phase two-pole filter with a cutoff frequency at 10 Hz, the KT method used a window size of $W = F_s/10$, and the DQPLL used PILF coefficients of $K_P = 0.15$ and $K_I = K_P^2/2$.

Single-axis methods used only $s_i[n]$ as the input. The SPE tracked the FF and harmonics at scales of [0.5, 1.5, 2.0], with the following design parameters: $g_\omega = 0.04$, $g_\phi = 0.004$, $g_m = 0.005$, $K_\alpha = 10$, and $z_\alpha = 0.9$. The APF used a windows size of $p = F_s/10$. The CWT used an $\omega_0 = 6.0$ and rejected any ridge in the TFR with a height less than 5000, which was experimentally determined.

A sequence of load transients were applied downstream from a PDW meter while the field and reference were measured. For the single-axis methods, Fig. 9 shows the transient performance of all methods, with the SPE and APF method being shown after the TVMAF post-processing step. Fig. 10 shows two-axis method transient performance, after TVMAF.

All three single-axis methods were able to track transients, with the APF showing the poorest transient performance and the SPE showing the most harmonic estimation error. The TVMAF was able to remove much, but not all, of the harmonic error and noise, at the cost of reduced transient tracking performance.

All three of the two-axis methods were stable and tracked the phase and frequency of the field. The three estimates were also drastically improved by the TVMAF, all dropping to lower

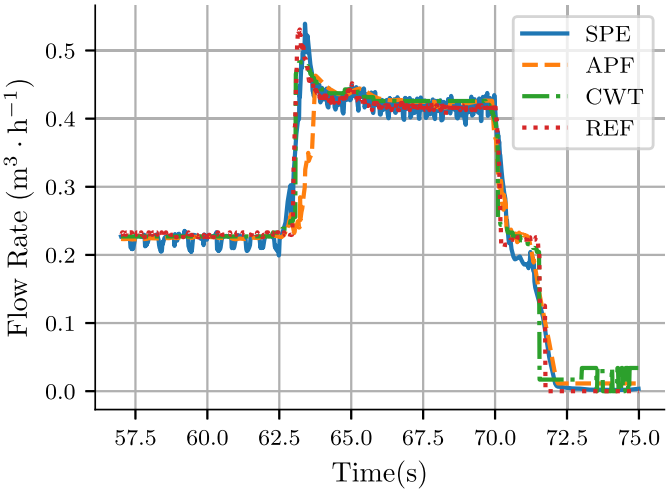

Fig. 9. Transient performance of single-axis methods.

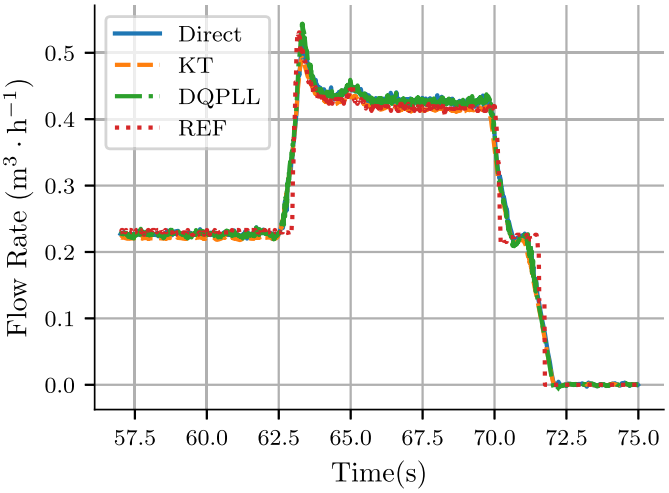

Fig. 10. Transient performance of two-axis methods.

error levels than all the single-axis methods while maintaining sharp transient responses.

As an estimate for computational requirements of the algorithms, and as a metric for choosing which method to use given application constraints, Fig. 11 plots L^2-Norm error v. computation time on our Intel ®Core i7-7600 CPU running at 2.8Ghz. All algorithms were performed on the same dataset, with padding added to bring the sample count to a power of two for handling edge effects as well as improving CWT computational efficiency.

These times are implementation-dependent, but they still serve as an estimate of computational complexity. As expected, the Direct and DQPLL estimation techniques take considerably less time than the KT method. Also as expected, the APF method takes longer and has more error than the SPE method, due to its higher computational-cost and poor transient performance. The CWT approach was the fastest single-axis method, mainly due to the computational efficiency of the FFT in convolving large power-of-two size datasets. Furthermore, since it tracks all the harmonics of the field simultaneously, it produces comparable error rates to the other methods without requiring a TVMAF.

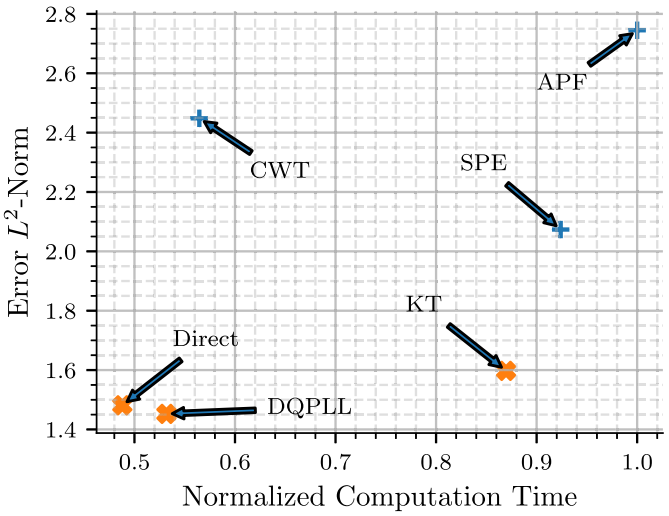

Fig. 11. Computation time vs. error.

A. Discussion

The two-axis estimation methods, in general, show higher stability, better transient performance, reduced harmonic modulation, and lower computational cost than the single axis methods. They are also applicable to a wider range of magnetic devices and flow rate sensing scenarios, such as those where back-flow through the meter is expected, because they can detect directionality of flow using the orthogonal magnetic components. Furthermore, the two-axis HEC compensation method has guaranteed stability and transient performance over the entire working range of the meter with a simpler implementation and looser tuning requirements [18]. This suggests the use of an at-least two-axis sensor that is aligned to two orthogonal magnetic field components. The Direct and DQPLL two-axis estimation methods showed the highest performance and smallest computational cost and as such are the recommended starting points for flow-rate extraction. The choice between the two will fall to accuracy and computational requirements.

If a two-axis sensor is not available, the single-axis SPE and CWT methods provide the highest accuracy and lowest computational cost. The CWT can be computed considerable faster due to its use of the FFT but will require a larger memory footprint. The SPE is more simply implemented and more accurately tracks transients but faces higher harmonic modulation error as well as spurious transients in the low flow regions. The choice between the two will be driven by the post-processing requirements of the application.

VII. Conclusion

This article presents a methodology and example system for non-contact flow rate extraction by retrofitting PDW meters that were previously only used for totalizing water consumption. This article provides models for the magnetic field produced by the magnetic couplers inherent to these meters, describes sensor selection and position, and also

presents methods for compensating the field measurements and extracting flow rate. Although this work considers PDW meters, the approach and estimation methods are agnostic to the specific meter and instead target any device that may exhibit a rotating magnetic field and can be viewed from the perspective of a nonideal magnetic encoder. Other situations might require alternative magnetic field models for different magnetic coupler structures, and/or different sensors capabilities to deal with sensitivity and sampling rate. This work in non-contact retrofit may also be expanded to apply to a wider range of magnetic devices using the techniques introduced here. Furthermore, this work is not restricted to devices containing permanent magnets or producing external magnetic fields as it only relies on the presence of an external sinusoidal field where frequency corresponds to the flow rate of some material through the device.

The experiments in this article on a popular style of water meter suggest the use of the HEC method and two-axis estimation methods. Computational burden is minimized while estimation accuracy is enhanced with the application of at least a two-axis sensor. Where possible, a three-axis sensor effectively provides a "compensation axis" that permits two clean quadrature rotation signals to be generated from a single, easily placed sensor package.

Acknowledgment

The authors gratefully acknowledge the valuable support of The Grainger Foundation. Eric A. Ponce also acknowledges the Alfred P. Sloan Foundation for its valuable support.

References

[1] M. Zhuang, M. Shahidehpour, and Z. Li, "An overview of non-intrusive load monitoring: Approaches, business applications, and challenges," in *Proc. Int. Conf. Power Syst. Technol. (POWERCON)*, Nov. 2018, pp. 4291–4299.

[2] J. Marais, R. Malekian, N. Ye, and R. Wang, "A review of the topologies used in smart water meter networks: A wireless sensor network application," *J. Sensors*, vol. 2016, pp. 1–12, Oct. 2016.

[3] C. Schantz, J. Donnal, B. Sennett, M. Gillman, S. Müller, and S. Leeb, "Water nonintrusive load monitoring," *IEEE Sensors J.*, vol. 15, no. 4, pp. 2177–2185, Apr. 2015.

[4] Y. Kim, T. Schmid, Z. M. Charbiwala, J. Friedman, and M. B. Srivastava, "NAWMS: Nonintrusive autonomous water monitoring system," in *Proc. 6th ACM Conf. Embedded Netw. Sensor Syst. (SenSys)*, New York, NY, USA, 2008, pp. 309–322.

[5] J. Fogarty, C. Au, and S. E. Hudson, "Sensing from the basement: A feasibility study of unobtrusive and low-cost home activity recognition," in *Proc. 19th Annu. ACM Symp. User Interface Softw. Technol. (UIST)*, 2006, pp. 91–100.

[6] C. Schantz, J. Donnal, S. Leeb, P. N. Marimuthu, and S. Habib, "WaterWOLF: Water watch on load flow," in *Proc. Urban Water II*, The Algarve, Portugal, May 2014, pp. 1–12.

[7] *T-10 Meter, Product Sheet*, Neptune Technol. Group, Tallassee, AL, USA, 2018.

[8] R. Ravaud, V. Lemarquand, and G. Lemarquand, "Analytical design of permanent magnet radial couplings," *IEEE Trans. Magn.*, vol. 46, no. 11, pp. 3860–3865, Nov. 2010.

[9] R. Ravaud, G. Lemarquand, V. Lemarquand, and C. Depollier, "Permanent magnet couplings: Field and torque three-dimensional expressions based on the Coulombian model," *IEEE Trans. Magn.*, vol. 45, no. 4, pp. 1950–1958, Apr. 2009.

[10] E. A. Ponce and S. B. Leeb, "A 3-D field solution for axially polarized multi-pole ring permanent magnets and its application in position measurement," *IEEE Trans. Magn.*, vol. 56, no. 3, pp. 1–9, Mar. 2020, doi: 10.1109/TMAG.2020.2966423.

[11] A. Sirohiwala and W. Bussing, "Advanced on-chip linearization in the A1335 angle sensor IC," Allegro Microsyst., LLC, Worcester, MA, USA, Tech. Rep. 296127-AN.

[12] *MLX90393 Triaxis Magnetic Node, MLX90393 Datasheet*, Melexis, Ypres, Belgium, Jan. 2020.

[13] S. Balemi, "Automatic calibration of sinusoidal encoder signals," *IFAC Proc. Volumes*, vol. 38, no. 1, pp. 68–73, 2005.

[14] Q. Lin, T. Li, and Z. Zhou, "Error analysis and compensation of the orthogonal magnetic encoder," in *Proc. 1st Int. Conf. Instrum., Meas., Comput., Commun. Control*, Oct. 2011, pp. 11–14.

[15] K. K. Tan and K.-Z. Tang, "Adaptive online correction and interpolation of quadrature encoder signals using radial basis functions," *IEEE Trans. Control Syst. Technol.*, vol. 13, no. 3, pp. 370–377, May 2005, doi: 10.1109/TCST.2004.841648.

[16] J. Lara and A. Chandra, "Position error compensation in quadrature analog magnetic encoders through an iterative optimization algorithm," in *Proc. 40th Annu. Conf. IEEE Ind. Electron. Soc. (IECON)*, Oct. 2014, pp. 3043–3048, doi: 10.1109/IECON.2014.7048943.

[17] K. Xiao and L. Wang, "Analysis and error compensation of electric sine/cosine encoder," in *Proc. 9th Int. Conf. Electron. Meas. Instrum.*, Aug. 2009, pp. 1–87, doi: 10.1109/ICEMI.2009.5274196.

[18] C. Albrecht, J. Klöck, O. Martens, and W. Schumacher, "Online estimation and correction of systematic encoder line errors," *Machines*, vol. 5, no. 1, p. 1, Jan. 2017, doi: 10.3390/machines5010001.

[19] "Closed loop position estimation with signal compensation for sinusoidal encoders with the ADMC401," Analog Devices, Norwood, MA, USA, Tech. Rep. AN401-23, 2000.

[20] Z. Zhang, C. Xiao, K. Yin, and H. Yan, "A magnetic field correction method for the non-ideally placed 3-axial magnetometer sensor," in *Proc. Int. Conf. Measuring Technol. Mechatronics Automat.*, Mar. 2010, pp. 130–133.

[21] S. Saliu, "Definition of instantaneous frequency on real signals," in *Proc. 10th Eur. Signal Process. Conf.*, 2000, pp. 1–4.

[22] B. Boashash, "Estimating and interpreting the instantaneous frequency of a signal. I. Fundamentals," *Proc. IEEE*, vol. 80, no. 4, pp. 520–538, Apr. 1992.

[23] S.-C. Pei and S.-G. Huang, "STFT with adaptive window width based on the chirp rate," *IEEE Trans. Signal Process.*, vol. 60, no. 8, pp. 4065–4080, Aug. 2012.

[24] T. Christopher and G. P. Compo, "A practical guide to wavelet analysis," *Bull. Amer. Meteorol. Soc.*, vol. 79, no. 1, pp. 61–78, Jan. 1998.

[25] X. Guo and M. Bodson, "Frequency estimation and tracking of multiple sinusoidal components," in *Proc. 42nd IEEE Int. Conf. Decis. Control*, vol. 5, Dec. 2003, pp. 5360–5365.

[26] B. Wu and M. Bodson, "Frequency estimation using multiple sources and multiple harmonic components," in *Proc. Amer. Control Conf.*, vol. 1, May 2002, pp. 21–22.

[27] B. Boashash, "Estimating and interpreting the instantaneous frequency of a signal. II. Algorithms and applications," *Proc. IEEE*, vol. 80, no. 4, pp. 540–568, Apr. 1992.

[28] L. Griffiths, "Rapid measurement of digital instantaneous frequency," *IEEE Trans. Acoust., Speech, Signal Process.*, vol. ASSP-23, no. 2, pp. 207–222, Apr. 1975.

[29] L. Qu, A. C. Kot, and S. H. Lum, "Comparative study of some discrete instantaneous frequency estimators," in *Proc. IEEE Singap. Int. Conf. Netw. Int. Conf. Inf. Eng.*, Jul. 1995, pp. 608–612.

[30] T. Emura and L. Wang, "A high-resolution interpolator for incremental encoders based on the quadrature PLL method," *IEEE Trans. Ind. Electron.*, vol. 47, no. 1, pp. 84–90, Feb. 2000.

[31] H. Van Hoang and J. W. Jeon, "Signal compensation and extraction of high resolution position for sinusoidal magnetic encoders," in *Proc. Int. Conf. Control, Automat. Syst.*, 2007, pp. 1368–1373.

[32] H. T. Le, H. Van Hoang, and J. W. Jeon, "Efficient method for correction and interpolation signal of magnetic encoders," in *Proc. 6th IEEE Int. Conf. Ind. Informat.*, Jul. 2008, pp. 1383–1388.

Eric A. Ponce received the B.S. and M.Eng. degrees from the Massachusetts Institute of Technology in 2017 and 2019, respectively, where he is currently pursuing the Ph.D. degree.

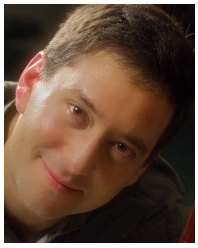

Steven B. Leeb (Fellow, IEEE) received the Ph.D. degree from the Massachusetts Institute of Technology in 1993. He has served as a Commissioned Officer of the USAF reserves. He has been a member of the M.I.T. Faculty with the Department of Electrical Engineering and Computer Science since 1993. He also holds a joint appointment at the MIT's Department of Mechanical Engineering. He is the author or coauthor of more than 150 publications and 20 U.S. patents in the fields of electromechanics and power electronics.

Peter A. Lindahl (Senior Member, IEEE) received the B.S. degree in electrical engineering from Penn State University, State College, PA, USA, in 2003, and the M.S. degree in electrical engineering and the Ph.D. degree in engineering from Montana State University, Bozeman, MT, USA, in 2009 and 2013, respectively. He joined as a Postdoctoral Associate with the Research Laboratory of Electronics, Massachusetts Institute of Technology, Cambridge, MA, USA, in 2014. He is currently a Senior Associate of Electrical Engineering and Computer Science Practice with Exponent, Inc., where he provides technical consulting services regarding energy and power systems, electromechanical machinery, sensors and instrumentation, and industrial controls.